Biosensors and Bioelectronics 130 (2019) 132–138

Contents lists available at ScienceDirect

Biosensors and Bioelectronics

journal homepage: www.elsevier.com/locate/bios

Integration of fluorescence imaging and electrochemical biosensing for both qualitative location and quantitative detection of cancer cells

Ya Cao, Yuhao Dai, Hong Chen, Yingying Tang, Xu Chen, Ying Wang, Jing Zhao*, Xiaoli Zhu*

Center for Molecular Recognition and Biosensing, School of Life Sciences, Shanghai University, 200444, PR China

ARTICLE INFO

Keywords:
DNA-templated silver nanoclusters
Fluorescent imaging
Electrochemical detection
ITO electrode
MCF-7 cell

ABSTRACT

In this work, DNA-templated silver nanoclusters (DNA-AgNCs) with unique fluorescent and electrochemical properties are prepared as dual signal probes for both qualitative imaging and quantitative detection of cancer cells in an integrated system. ITO electrode that has good light transmittance and electric conductivity is employed as a substrate for dual analysis of cancer cells. ITO electrode is firstly modified by AS1141 aptamer, which could selectively bind to nucleolin overexpressed on the surface of a model breast cancer cell, MCF-7 cell line. The composite of mucin 1 antibody (anti-MUC1) and DNA-AgNCs then binds to MUC1 on the surface of captured MCF-7 cell, forming a sandwich-like structure. Therefore, our method allows noninvasive fluorescence imaging and amplified electrochemical detection using a single labeling platform, providing a biocompatible and highly specific method for adequate analysis of cancer cells. Experimental results demonstrate that strong red fluorescence of DNA-AgNCs clearly displays the loading of cancer cells on ITO electrode after dual recognition, and amplified electrochemical signals of DNA-AgNCs enable improved sensitivity toward quantitative analysis with a detection limit of 3 cells.

1. Introduction

Cancer is a major public health problem that seriously threatens human health all over the world, and pathological examination of tumor tissues is known as the gold standard of cancer diagnosis in clinic (Bray et al., 2018). However, tumor heterogeneity raises a big challenge to cancer diagnosis, as molecular profiling varies from site to site with different disease progression (Alizadeh et al., 2015; Koren and Bentires-Alj, 2015). In this sense, precise identification of cancer cells is of great need for tumor profile before the performance of effective cancer treatment (Aceto et al., 2014; Chinen et al., 2015; Li et al., 2007). On the other hand, circulating tumor cells (CTCs) that escape from primary tumor are believed as the beginning of tumor metastasis and may eventually lead to cancerous death (Joosse et al., 2015; Maheswaran and Haber, 2015; Mohme et al., 2017). Although CTCs as potent targets of "liquid biopsy" are able to provide detailed information about tumor metastasis and disease progression, extremely-low number in blood is still the major trouble in isolation, detection and classification of CTCs in practice (Huang et al., 2018; Stoecklein et al., 2016). To address above-mentioned problems, simple but effective platform is always required to allow adequate analysis of cancer cells for efficient cancer diagnosis and management.

To date, fluorescence imaging and electrochemical techniques are the two most popular modes for analysis of cancer cells. On the one hand, a great advance has been made in higher-quality fluorescence imaging of cancer cells incorporating with confocal microscopy and even stimulated emission depletion microscopy, which enables direct visualization of cancer cells with abundant location information (Fan et al., 2016; Kelley et al., 2017; Tao et al., 2017). Even so, fluorescent imaging techniques as semi-quantitative techniques are not able to satisfy the demand of highly sensitive measurement. On the other hand, electrochemical techniques have demonstrated ultra-high sensitivity and accuracy in quantitative detection of breast, prostate, liver and cervical cancer cells. However, they are usually not intuitive for quite limited locational information (Sun et al., 2018; Wan et al., 2014; Zhao et al., 2018). Although fluorescence imaging and electrochemical techniques are most of the time compared, their integration may help to decrease false-positive and negative results and provide more comprehensive and valuable information for cancer cell analysis.

As an appealing fluorescent probe, DNA-templated silver nanoclusters (DNA-AgNCs) possess stronger fluorescence emission and higher photostability than conventional fluorescent dyes and also have better biocompatibility and less blinking problems than quantum dots, thereby attracting increasing attention in cell imaging (Li et al., 2018; Zhang et al., 2018). For example, Jiang et al. realized cancer cell imaging based on fluorescence resonance energy transfer between

* Corresponding authors.
E-mail addresses: jingzhao@t.shu.edu.cn (J. Zhao), xiaolizhu@shu.edu.cn (X. Zhu).

https://doi.org/10.1016/j.bios.2019.01.024
Received 20 November 2018; Received in revised form 9 January 2019; Accepted 17 January 2019
Available online 18 January 2019
0956-5663/

DNA-AgNCs and single-walled carbon nanotubes (Jiang et al., 2015), while Wang and co-workers developed a cancer cell imaging strategy using fluorescence enhancement of DNA-AgNCs by G-quadruplex (Zhu et al., 2015). At the meanwhile, DNA-AgNCs are also simple but practical sources of amplified electrochemical signals, benefiting from unique advantages of electrochemical techniques in ultra-sensitive quantification of metal component (Miao et al., 2015; Peng et al., 2018). For example, Chen et al. proposed a "turn-on", label-free and sensitive electrochemical strategy based on hybridization chain reactions and DNA-AgNCs (Chen et al., 2015). Besides, Hu et al. developed a novel electrochemical assay for label-free detection of TdT activity based on electro-catalytic activity of the DNA-AgNCs (Hu et al., 2017). The unique fluorescence and electrochemical properties make DNA-AgNCs become a type of valuable dual-signal probe, which has not been intensively explored yet.

Given the advantages of DNA-AgNCs in both fluorescent imaging and electrochemical detection, we herein propose a simple but effective method for both qualitative and quantitative analysis of cancer cells by using breast cancer cell MCF-7 as an example. Two representative tumor markers nucleolin (NCL) and mucin 1 (MUC1) were chosen to identify MCF-7 cells. NCL is a bcl-2 mRNA binding protein over-expressed in active breast cancer, while over-express of MUC1 is closely related to the metastasis of breast cancer (Gendler, 2001; Nath and Mukherjee, 2014; Wolfson et al., 2018). Fig. 1A describes the preparation of dual-signal DNA-AgNCs. A G-rich sequence is used as a template to mediate the synthesis of AgNCs in the presence of ammonium acetate (NH_4Ac), silver nitrate ($AgNO_3$) and sodium borohydride ($NaBH_4$) (Zhu et al., 2015). Fig. 1B further describes the preparation of (anti-MUC1 antibody)-(DNA-AgNCs) conjugate (CADA). Maleimide-activated anti-MUC1 antibody is prepared through the connection of amine-containing anti-MUC1 and the crosslinker Sulfo-SMCC, which further reacts with sulfhydryl groups on DNA-AgNCs. Fig. 1C illustrates the principle of our method. Indium tin oxide (ITO) electrode, a widely-used substrate for cell capture, is utilized here because of excellent light transmission, good conductivity, and stable electrochemical and physical properties (Aydın and Sezgintürk, 2017; Wu et al., 2013; Zhang et al., 2016). ITO electrode is firstly functionalized by AS1141 aptamer, which then selectively binds to NCL overexpressed on the surface of MCF-7 cells with high affinity. Then, a sandwich-like structure is formed at ITO electrode through the binding of CADA on the surface of captured MCF-7 cells. Experimental results validate that MCF-7 cells can be imaged by confocal microscopy using strong fluorescence emission of DNA-AgNCs and quantitatively determined using amplified electrochemical signal of DNA-AgNCs.

2. Experimental section

2.1. Reagents and materials

All oligonucleotides (SH-DNA: 5′-SH-C_6-T(20)-ATATAATTCCCACC CAC-3′; AS1411: 5′-GGTGGTGGTGGTTGTGGTGGTGGTGG-T_6-NH_2–3′; FAM-AS1411: 5′-FAM-GGTGGTGGTGGTTGTGGTGGTGGTGG-T_6-NH_2–3′) were synthesized by Sangon Biotechnology Co., Ltd. (Shanghai, China). ITO electrode was purchased from Tianjin Aida Hengyi Technology Development Co., Ltd. (Tianjin, China). (3-aminopropyl)triethoxysilane (APTES), NH_4Ac, $AgNO_3$, $NaBH_4$ and bovine serum albumin (BSA) were obtained from Sigma-Aldrich. Anti-MUC1 was purchased from Abcam Trading Co., Ltd. (Shanghai, China). Glutaraldehyde and Sulfo-SMCC were purchased from Aladdin Industration Co., Ltd. (Shanghai, China). 30 K Ultrafiltration centrifuge tube (0.5 mL) was purchased from Shanghai Advantage Biological Co., Ltd. (Shanghai, China). HepG2, MDA-MB-231, L-02 and MCF-7 cells were purchased from the Institute of Biochemistry and Cell Biology of Chinese Academy of Science (Shanghai, China). DMEM and RPMI-1640 medium were purchased from Gibco Co., Ltd. (Beijing, China). Hoechst and Trypsin-EDTA Solution were purchased from Jiangsu Keji Biotechnology Co., Ltd. (Nanjing, China). All solutions were prepared with Milli-Q water (18.2 MΩ cm^{-1}) from a Milli-Q purification system (MA, America). All other chemicals were of analytical reagent grade.

2.2. Preparation of AS1411-functionalized ITO electrode (AS1411/ITO)

ITO substrate was cleaned by sequential sonication in neat acetone for 20 min, ethanol for 15 min and distilled water for 30 min, which was

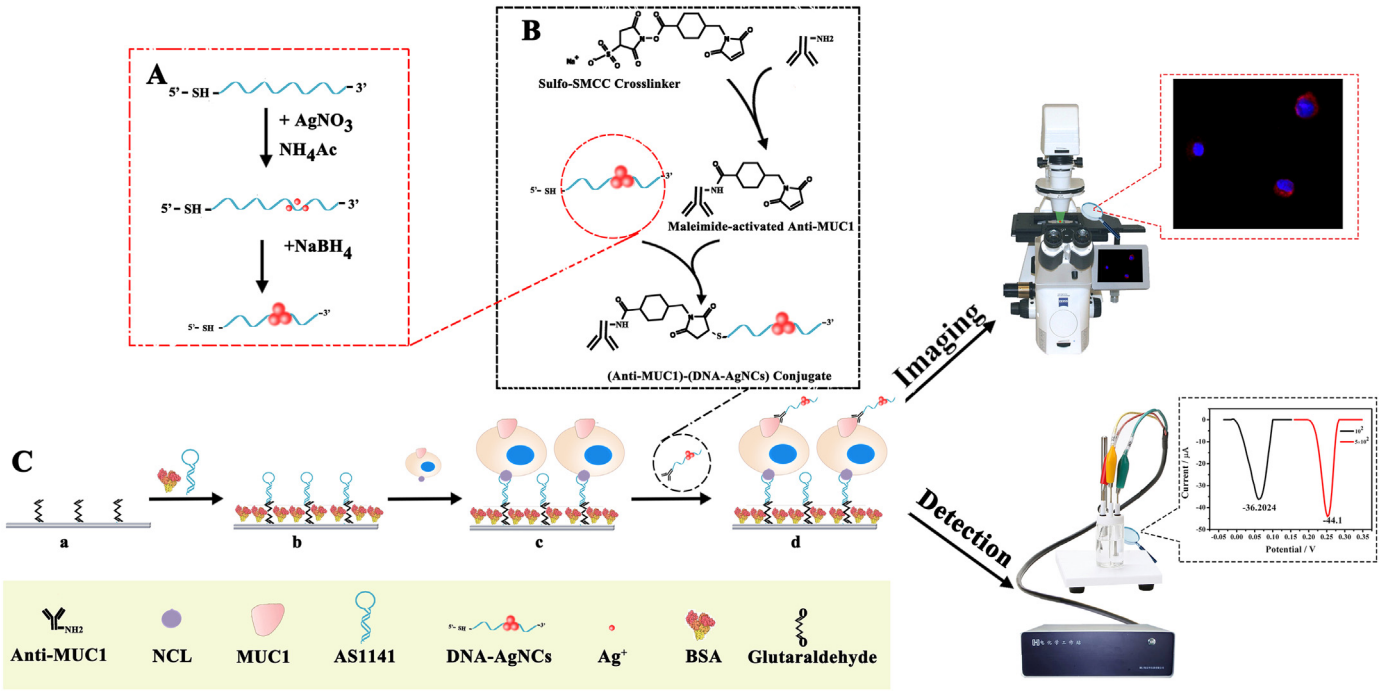

Fig. 1. (A) The synthesis process of DNA-AgNCs; (B) Cross-linking process of Anti-MUC1 and DNA-AgNCs; (C) Schematic illustration for mechanisms of qualitative imaging and quantitative detection by using DNA-AgNCs as fluorescent and electrochemical probe.

followed by being rinsed with ultrapure water and dried in nitrogen atmosphere. After then, the substrate was dipped in an ethanol solution of 5% APTES overnight in order to yield high-roughness polymerized aminosiloxane films. After being rinsed with ethanol, the ITO electrode was immediately transferred to 80 °C hot water for 10 min to remove loosely bound APTES molecules, which was then dried in nitrogen atmosphere. Then, the electrode was incubated with 500 μL of glutaraldehyde at 37 °C for 1.5 h, which was well rinsed three times with PBS. After being dried with nitrogen atmosphere, 2 μM of AS1411 aptamer was added to the pretreated ITO electrode at room temperature for 1.5 h, which was followed by sealing with 2% BSA for 1 h at 37 °C. Finally, AS1411/ITO was prepared for further use. The surface density of immobilized AS1411 aptamer was estimated by chronocoulometric measurement based on the assumption that redox active hexaammineruthenium(III) cation associates with anionic phosphate backbone of DNA (Steel et al., 1998).

2.3. Preparation of DNA-AgNCs

The synthesis of DNA-AgNCs was based on previous report (Zhu et al., 2015). Firstly, 20 mM of NH_4Ac (95 μL) was mixed with 100 μM of $AgNO_3$ (100 μL) and 100 μM of SH-DNA (5 μL) to prepare a solution with the total volume of 200 μL. Followed by vigorous shaking, the solution was kept at 4 °C in dark for 20 min. After then, 100 μM of $NaBH_4$ solution (5 μL) was added to the above solution, which was followed by vigorous shaking. The color of the solution changed gradually to yellow for the formation of DNA-AgNCs. Stable DNA-AgNCs solution was obtained after about 2 h, and the fluorescence was observed by GelDoc XR^+ Molecular Imager (Bio-Rad, Chicago, America).

2.4. Preparation of CADA

To prepare a compound of anti-MUC1 and DNA-AgNCs, 1.3 μM of anti-MUC1 (8 μL) and 10 μM of sulfo-SMCC (5.4 μL) were dissolved in 85 μL of PBS solution simultaneously and reacted at 25 °C for 2 h. Then, it was transferred to a 30 K ultrafiltration centrifuge tube to be centrifuged at 14,000 r/min for 10 min. The upper unfiltered substance was collected and re-dissolved in 100 μL of PBS. After then, the prepared DNA-AgNCs were added to the above unfiltered substance and reacted at 25 °C for 2 h. The fully reacted solution was transferred to a 30 K centrifuge tube and the centrifugation step was repeated. Finally, the upper CADA was re-dissolved in 200 μL of serum-free medium for further use.

2.5. Cell capture on the surface of ITO electrode

HepG2 and MCF-7 cells were cultured in DMEM medium supplemented with 10% FBS, 80 U/mL penicillin and 0.08 mg/mL streptomycin. MDA-MB-231 and L-02 cells were cultivated in RPMI-1640 medium supplemented with 10% FBS, 80 U/mL penicillin and 0.08 mg/mL streptomycin. All the cells were maintained in a humidified incubator at 37 °C with 5% CO_2 and 80% relative humidity, and were detached from the culture surface by trypsinization and were collected by centrifugation at 2000 rpm for 5 min. After being washed with PBS buffer twice, the cell sediment was dispersed in the buffer at various concentrations. Cell number was quantitated using TC20TM Automated Cell Counter (Bio-Rad, America). After then, the harvested cells were reacted with ITO electrode at 37 °C for 2 h in order to be captured.

2.6. Cell analysis and imaging

For MTT assay, MCF-7 cells were seeded in 96-well plates at a density of 1.0×10^4 cells/mL and allowed to incubate overnight before treatments. After that, 70 μL of DMEM medium and 30 μL of the centrifuged AgNCs (7.5 μM) were added to the experimental group, and reacted at 37 °C for 2.5 h. Then, MCF-7 cells were incubated with MTT (50 μL) at 37 °C for 2.5 h, followed by adding 150 μL of DMSO and keeping for 10 min. The ultraviolet absorption was determined at 550 nm using the microplate spectrophotometer system (Spectra max190-Molecular Devices). To prove the recognition ability of CADA on MCF-7 cells, cell nucleus was firstly stained with Hoechst for 15 min, and was then incubated with CADA for 45 min. The images of ITO electrode were obtained by using a LSM 710 confocal laser scanning microscope (Zeiss, Germany) with 345 nm and 550 nm of excitation wavelengths and 478 nm and 610 nm of the corresponding emission wavelengths.

2.7. Electrochemical detection

All electrochemical measurements were conducted on a CHI-660C electrochemical workstation (CH Instruments, Shanghai, China) at room temperature with a conventional three-electrode system, which involves the ITO electrode as the working electrode, a saturated calomel electrode (SCE) as the reference electrode, and a platinum wire as the auxiliary electrode. Linear sweep voltammetry (LSV) measurement was performed in 1 M KCl solution with the potential from −0.3 to 0.5 V. Electrochemical impedance spectroscopy (EIS) measurement was performed in 0.1 M KCl solution contained 5 mM $[Fe(CN)_6]^{3-/4-}$ with the biasing potential of 0.224 V in the frequency range from 0.01 Hz to 10 kHz.

3. Results and discussion

3.1. Characterization of DNA-AgNCs

We firstly studied fluorescent and electrochemical properties of synthesized DNA-AgNCs. A typical transmission electron microscopy (TEM) image clearly displayed that the DNA-AgNCs were uniform with an average diameter of around 2 nm (Fig. S1A in Supporting information). The fluorescence image and fluorescent spectrum of DNA-AgNCs are shown in Figs. S1B and S1C. Obviously, after reduction of silver ions on DNA template, DNA-AgNCs showed a strong fluorescent intensity with emission wavelength at 575 nm. The fluorescent characterization of DNA-AgNCs is in good agreement with previous report (Li et al., 2018; Zhang et al., 2018). As shown in Fig. S1D, condition optimization experiment further revealed that the fluorescent intensity was time-dependent and a high enough intensity was obtained after 2 h. Fig. S1E displays the electrochemical response of DNA-AgNCs in the solution. A high peak current was observed at the potential of 0.06 V, which was ascribed to the solid-state Ag/AgCl process and thus demonstrated satisfactory electro-activity of DNA-AgNCs. Overall, DNA-AgNCs were proven with excellent fluorescent and electrochemical properties, suggesting potential application in both fluorescent imaging and electrochemical detection.

3.2. Capture and labeling of MCF-7 cells on ITO electrode

The capture and labeling of MCF-7 cells at an ITO electrode was firstly confirmed by EIS. Fig. S2 displays EIS characterization of stepwise modifications at an ITO electrode. A small impedance was obtained at a bare ITO electrode, suggesting feasible approach of electroactive $[Fe(CN)_6]^{3-/4-}$ to electrode surface (curve a). The electrode was then modified with APTES. In this case, even smaller impedance was noted (curve b). This would be attributed to the positively charged amine groups presented on the electrode surface, confirming the formation of a SAM of APTES (Mishra et al., 2013). Increased surface impedance was observed after immobilization of AS1411 aptamer, which was ascribed to electrostatic repulsion between DNA molecules and electro-active probes (curve c). To further confirm the conjugation of AS1411 aptamer, fluorescent dye labeled aptamer (FAM-AS1411) was utilized as an indicator. As shown in Fig. S2B, green fluorescence could be observed when APTES-modified ITO electrode was treated

with FAM-AS1411, revealing the successful immobilization of AS1411 aptamer through crosslinking with glutaraldehyde. The surface density of the immobilized AS1411 aptamer was estimated to be 2.62×10^{12} molecules/cm^2 by using a classical method (Steel et al., 1998). Another increase of impedance was observed after the capture of MCF-7 cells, since steric hindrance of captured MCF-7 cells strongly prevented electro-active probes from approaching to electrode surface (curve d). When CADA bound to the surface of captured MCF-7 cells, a quite large increase of surface impedance was obtained (curve e). This apparent increment can be rationalized in terms of (i) the presence of significant steric effect induced by anti-MUC1 antibody and (ii) the increase in electrostatic repulsion towards $[Fe(CN)_6]^{3-/4-}$ due to the negatively charged phosphate backbone of DNA in DNA-AgNCs. Therefore, EIS studies verified the capture and labeling of MCF-7 cells through dual recognition of over-expressed NCL and MUC1.

To prove nondestructive and biocompatible properties of surface capture and cell labeling, we studied cell viability using MTT assay. NAD(P)H-dependent oxidoreductase enzymes involved in live cells catalyze the conversion of MTT to the insoluble formazan, so MTT assay is able to reveal cell viability by measuring absorbance value at 500 nm using UV–vis spectrometry (Kim et al., 2009). As shown in Fig. S1F, MCF-7 cells immobilized on an ITO electrode before and after treatment with CADA were measured as the experimental groups, while MCF-7 cells incubated on a bare ITO electrode overnight were used as the control. As expected, both the two experimental groups displayed comparable high cell viability as the control. Therefore, the results demonstrated that neither interaction with AS1411 aptamer nor interaction with CADA had any negative effect on cell viability, suggesting the potential for non-destructive imaging and analysis of cancer cells using our method.

3.3. Fluorescence imaging of surface-captured MCF-7 cells

After confirmation of the capture and subsequent labeling of MCF-7 cells at an ITO electrode, we conducted confocal fluorescence imaging of captured cells using Hoechst dyes and DNA-AgNCs. Hoechst dyes with blue fluorescence are usually used to examine live cells as a type of supravital staining. As shown in Fig. 2A, blue fluorescence of Hoechst dyes clearly indicated cell viability of surface attached MCF-7 cells at ITO electrode. At the meantime, strong red fluorescence from DNA-AgNCs was also observed that overlapped most of the area with blue fluorescence in the merge image. The fluorescent results demonstrated that DNA-AgNCs possessed strong enough intensity for imaging of MCF-7 cells at ITO electrode. Fig. 2B shows enlarged fluorescence images of the surface-captured cells after labeling with DNA-AgNCs. Obviously, strong red fluorescence was observed at the same area with blue fluorescence of Hoechst dyes. The merge image further indicated that red fluorescence surrounded extracellular surface, providing locational information of both membrane protein MUC1 and immobilized MCF-7 cells. Fig. S2 further displays fluorescent images after incubation with CADA for different time. 45 min was chosen as optimized time, as the fluorescent composites could across cell membrane and entered into the cells after longer time incubation (60 min).

Confocal fluorescence images in the presence of different amounts of MCF-7 cells were then measured by using Hoechst dyes and DNA-AgNCs. It can be seen from Fig. 3A that DNA-AgNCs emitted strong red fluorescence to image surface-attached MCF-7 cells at ITO electrode, which had substantial overlap with blue fluorescence after Hoechst staining. The fluorescent region was found to reduce with the decrease of cell number. The images using our method were in good agreement with that using conventional staining, reconfirming that CADA effectively recognized and bound to AS1411-captured MCF-7 cells at ITO electrode. Fig. 3B further reveal the relative fluorescent intensities in the presence of different amount of MCF-7 cells by setting fluorescent intensity of 10^5 MCF-7 cells as 100%. The fluorescence intensities were concentration-dependent, which decreased with the decrease of cell number. Overall, fluorescent results demonstrated excellent performances of our method in imaging surface-attached cells through dual recognition.

3.4. Electrochemical amplified detection of surface-captured MCF-7 cells

To realize quantitative measurement of target cells, we employed electrochemical technique for amplified detection of surface-captured

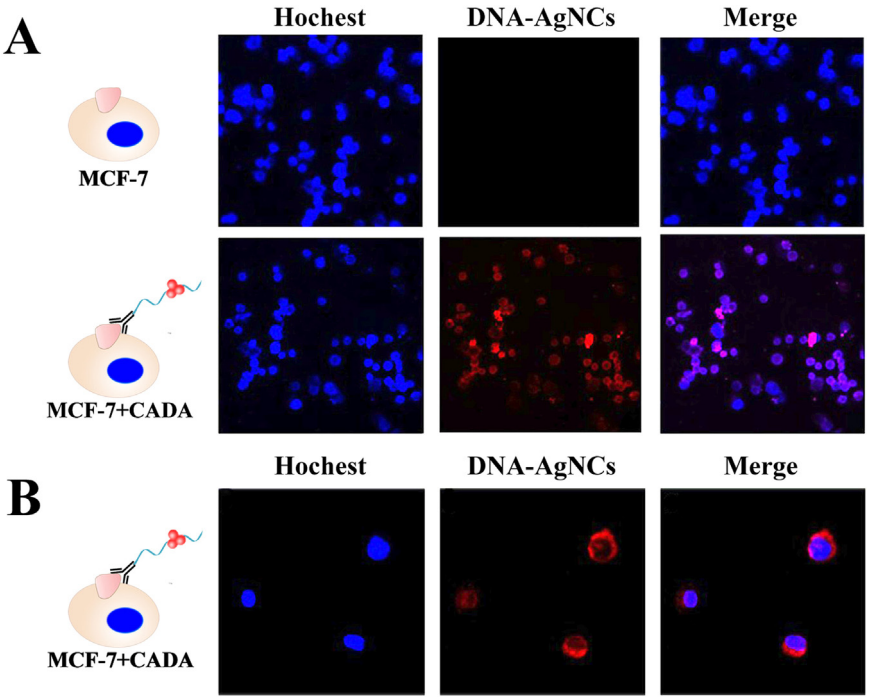

Fig. 2. (A) Confocal fluorescence images of MCF-7 cells with or without the incubation of CADA. (B) Enlarged fluorescent images of MCF-7 cells with the labeling of DNA-AgNCs. Hoechst dyes and DNA-AgNCs contribute to blue and red fluorescence, respectively.

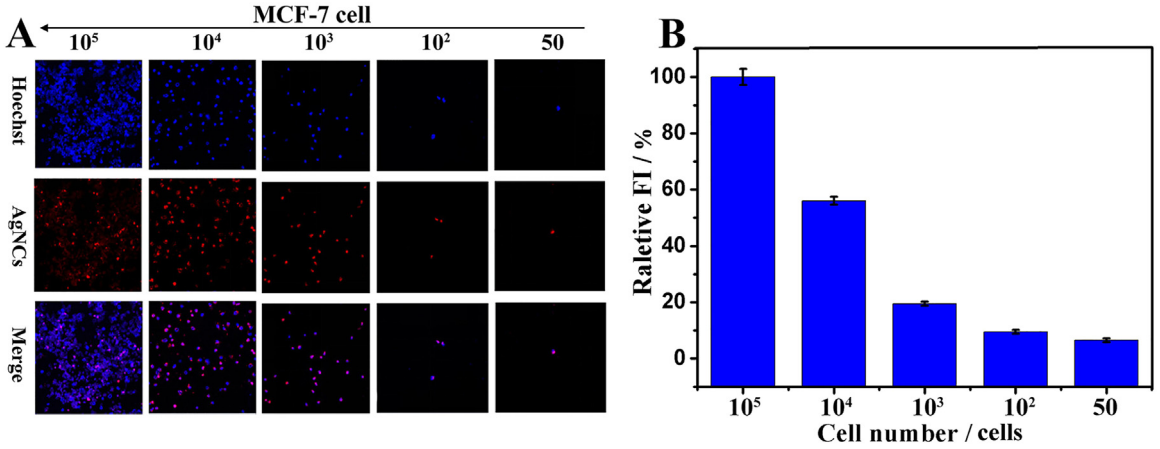

Fig. 3. Confocal fluorescent images of MCF-7 cells with different cell numbers (50, 10^2, 10^3, 10^4 and 10^5 cells) using Hoechst and DNA-AgNCs. (B) Relative fluorescence intensities (FIs) measured by ImageJ software for different numbers of MCF-7 cells.

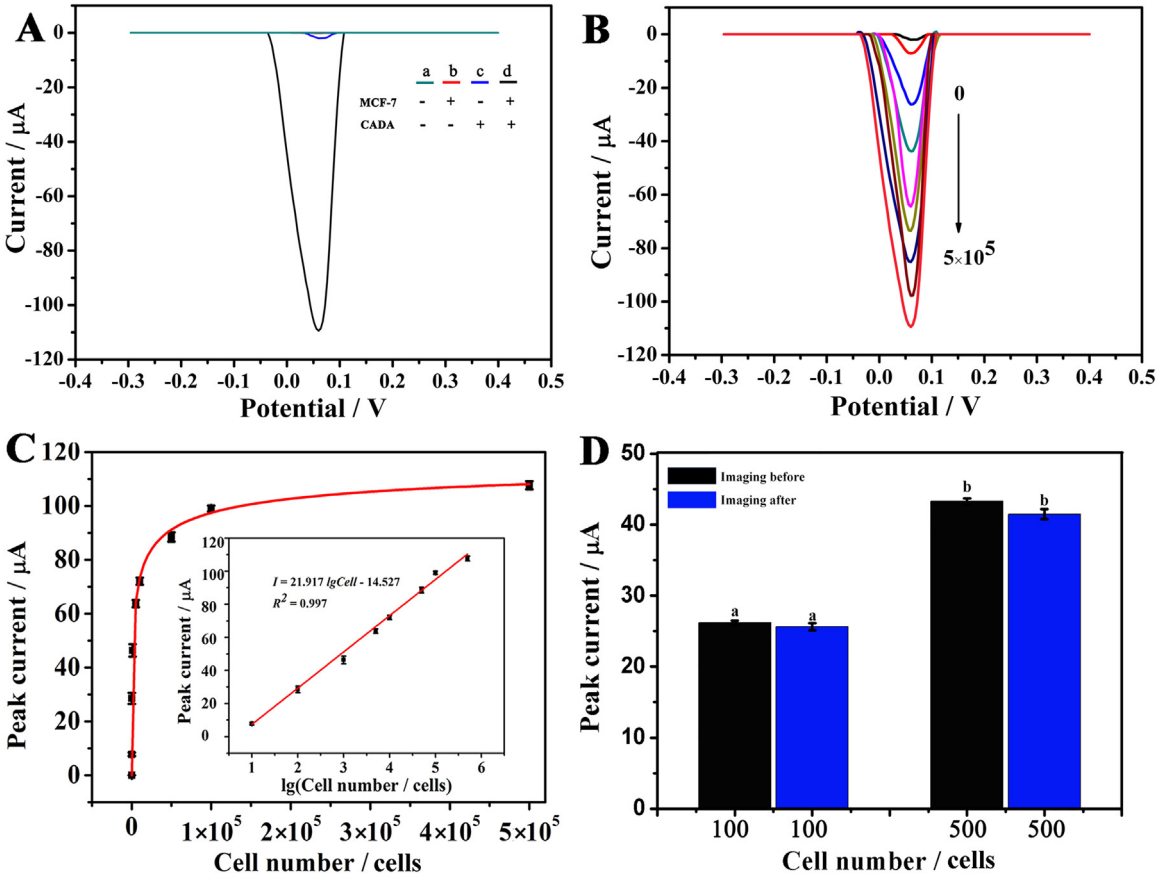

Fig. 4. (A) LSV responses and schematic illustration (inset) of ITO electrode at the different conditions: (a) AS1141/ITO; (b) AS1141/ITO treated with MCF-7 cells; (c) AS1141/ITO treated with CADA and (d) AS1141/ITO treated with MCF-7 cells and CADA in sequence. It should be noted that curve a and curve b coincides with each other. (B) LSV responses for the detection of MCF-7 cells with different amounts: 0, 10, 10^2, 10^3, 5×10^3, 10^4, 5×10^4, 10^5 and 5×10^5; (C) Peak current values versus different cell numbers. Inset: The linear relationship between peak current values and the logarithmic values of cell numbers. (D) Comparison of peak current values for the detection of MCF-7 cells before (black column) and after (red column) fluorescence imaging. Columns with different alphabet are significantly different ($p \leq 0.05$).

MCF-7 cells using DNA-AgNCs as a signal source. Fig. 4A illustrates electrochemical results after different modifications at ITO electrode. Quite low electrochemical responses were obtained for AS1411/ITO and that after the capture of MCF-7 cells or that after reaction with DNA-AgNCs without MCF-7 cells (curves a-c), while much higher electrochemical response was obtained after the capture of MCF-7 cells and incubation of CADA. The electrochemical response showed a similar peak potential (0.06 V) as that in electrochemical characterization of DNA-AgNCs (Fig. S1E), ascribing to oxidation of immobilized DNA-AgNCs at ITO electrode. The electrochemical results are consistence with our expectation. Lack of DNA-AgNCs at AS1411/ITO and that incubated with target cells prohibited the produce of electrochemical response, while non-specific adsorption of DNA-AgNCs in the absence of target cells only aroused negligible low signal. After dual

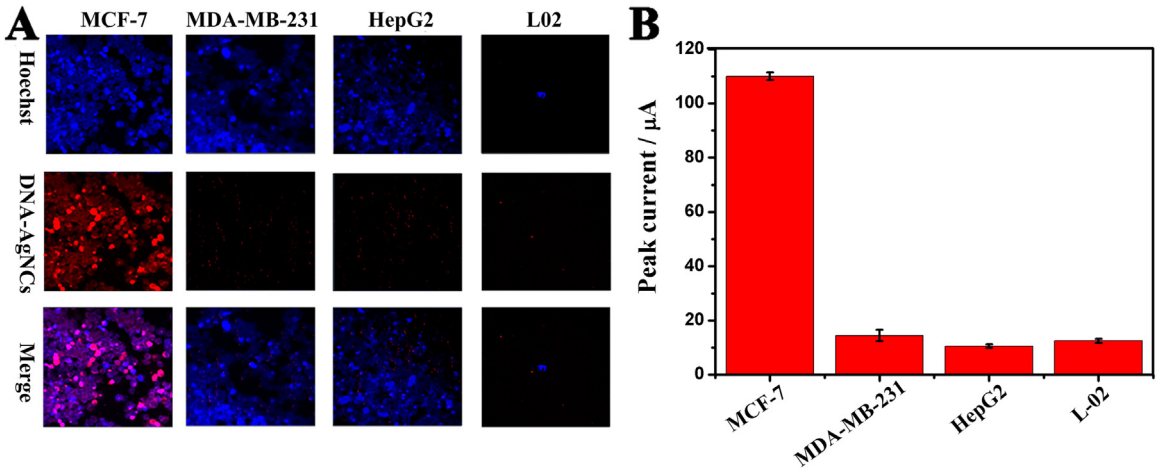

Fig. 5. (A) Fluorescence images of different cells using Hoechst and DNA-AgNCs, respectively; (B) The peak current in the presence of different cells including MCF-7, MDA-MB-231, HepG2 and L-02. All cell amounts are 5×10^5 cells.

recognition on MCF-7 cells, DNA-AgNCs were loaded on the electrode surface and promoted the produce of electrochemical signal via the solid-state Ag/AgCl process. Therefore, the electrochemical results verified the feasibility of our method in quantitative detection of MCF-7 cells.

Fig. 4B further reveals the electrochemical responses in the presence of different amounts of target cells. Electrochemical responses from surface-attached DNA-AgNCs increased with the addition of cell amount, because increased amount of captured cells led to the corresponding increase of binding of CADA, resulting in the enhanced accumulation of DNA-AgNCs onto the electrode surface. Fig. 4C displays the relationship between peak current and cell amount, showing similar tendency as that in Fig. 5B. The inset figure further demonstrated a linear relationship between peak current and the logarithm of cell number in a range from 10 to 5×10^5 cells with a linear equation $I = 21.917\ lgC_{cell} - 14.527$ ($R^2 = 0.997$) and a quite detection limit of 3 cells. Meanwhile, the electrochemical experiments have been conducted three times and the detection precision has been evaluated, giving an average *RSD* value of 3.57%. The results signify acceptable reproducibility and precision of the established method.

In our method, DNA-AgNCs can be used a type of dual-signal probe in both fluorescence imaging and electrochemical detection, so we wonder whether fluorescence imaging has any negative effect on the electrochemical detection. Fig. 4D shows electrochemical responses with or without the performance of fluorescence imaging. In the presence of two different amounts (100 and 500 cells) of MCF-7 cells, the electrochemical responses after fluorescent imaging were all comparable to those without fluorescence imaging. Overall, the results not only reconfirmed satisfactory biocompatibility of our method to maintain the cell viability after dual recognition, but also suggested dual signals of DNA-AgNCs that allowed the simultaneous achievement of noninvasive fluorescence imaging and amplified electrochemical detection.

3.5. Specificity studies of our method

Beside high sensitivity, high specificity is also an important parameter to evaluate practicality of an analytical method. Several different cells were used as control to demonstrate the specificity of our method, including HepG2, L-02 and MDA-MB-231 cells. Fig. S3 displays flow cytometry analysis of different cells. Both NCL and MUC1 expressions in MCF-7 were positive, the expression of NCL in HepG2 and MBA-MD-231 cells was positive and the expression of MUC1 was negative, and both protein expressions in L-02 were negative. Fig. 5A firstly exhibited fluorescence images at ITO electrodes in the presence of different cells. A strong red fluorescence from DNA-AgNCs was observed in the presence of MCF-7 cells, while nearly no fluorescent signals were observed in the presence of other control cells. The fluorescence images of DNA-AgNCs labeling were superior to that using Hoechst staining. Red fluorescence was only observed after dual recognition, while blue fluorescence of Hoechst dye was observed even after single recognition. Fig. 5B further shows electrochemical results in the presence of different cells. Similar as that in fluorescence images, a quite high electrochemical response was obtained in the presence of MCF-7 cells while extremely low electrochemical responses were obtained in the presence of control cells. Overall, both fluorescent and electrochemical analysis confirmed high specificity of our method due to dual signal-assisted dual recognition. Moreover, the usability of our method in real sample was also evaluated. To this end, serum samples were prepared by adding different amounts (100, 1000 and 10,000) of MCF-7 cells into human serum and analyzed as outlined above. As shown in Fig. S5, both fluorescence imaging and accurate electrochemical detection of cancer cells were successfully realized, indicating a favorable feasibility of our method for clinical use.

4. Conclusions

In summary, a quantitative imaging and quantitative detection system was designed based on electrochemical and fluorescent dual signals of DNA-AgNCs. Introduce of DNA-AgNCs and the preparation of CADA were critical to the success of this design, while dual recognition of NCL and MUC1 on the surface of MCF-7 cell successfully enabled the specificity of the system. By integrated the advantages of DNA-AgNCs and ITO electrodes, imaging and sensitive detection of MCF-7 cells was achieved with a detection limit of 3 cells. The system of cell capture and labeling had good biocompatibility for cancer cells, which has been confirmed by MTT. Therefore, the integration of noninvasive fluorescence imaging and amplified electrochemical detection using a simple labeling platform was established. It provides an important basis for the detection and analysis of trace cancer cells in the future. Certainly, there still exist limitations in this principle-of-proof system. For example, the response signal may be disturbed by the coexistence of target MCF-7 cells and non-target NCL-positive cancer cells. Nevertheless, with the rapid development of Cell-SELEX techniques (Tan et al., 2013), this issue will be effectively solved by using more specific aptamers that are able to bind to a certain cell line instead of AS1411 aptamer, which is an ongoing subject of interest in our lab.

Acknowledgments

This work was supported by the National Natural Science

Foundation of China (Grant Nos. 81871449, 81671781 and 21575088).

Credit author statement

Y. Cao designed the study, performed the experiments and wrote the manuscript.

Y.H. Dai and H. Chen analyzed the data and performed the electrochemical experiments.

Y.Y. Tang, X. Chen and Y. Wang performed the fluorescence imaging experiments.

J. Zhao and X.L. Zhu supervised the study, interpreted the data and wrote the manuscript.

All authors reviewed, edited and approved the manuscript.

Declaration of interests

None.

Appendix A. Supplementary material

Supplementary data associated with this article can be found in the online version at doi:10.1016/j.bios.2019.01.024.

References

Aceto, N., Bardia, A., Miyamoto, D.T., Donaldson, M.C., Wittner, B.S., Spencer, J.A., Yu, M., Pely, A., Engstrom, A., Zhu, H., Brannigan, B.W., Kapur, R., Stott, S.L., Shioda, T., Ramaswamy, S., Ting, D.T., Lin, C.P., Toner, M., Haber, D.A., Maheswaran, S., 2014. Cell 158, 1110–1122.

Alizadeh, A.A., Aranda, V., Bardelli, A., Blanpain, C., Bock, C., Borowski, C., Caldas, C., Califano, A., Doherty, M., Elsner, M., Esteller, M., Fitzgerald, R., Korbel, J.O., Lichter, P., Mason, C.E., Navin, N., Pe'er, D., Polyak, K., Roberts, C.W., Siu, L., Snyder, A., Stower, H., Swanton, C., Verhaak, R.G., Zenklusen, J.C., Zuber, J., Zucman-Rossi, J., 2015. Nat. Med. 21, 846–853.

Aydın, E.B., Sezgintürk, M.K., 2017. Trends Anal. Chem. 97, 309–315.

Bray, F., Ferlay, J., Soerjomataram, I., Siegel, R.L., Torre, L.A., Jemal, A., 2018. CA Cancer J. Clin. 0, 1–31.

Chen, L., Sha, L., Qiu, Y., Wang, G., Jiang, H., Zhang, X., 2015. Nanoscale 7, 3300–3308.

Chinen, A.B., Guan, C.M., Ferrer, J.R., Barnaby, S.N., Merkel, T.J., Mirkin, C.A., 2015. Chem. Rev. 115, 10530–10574.

Fan, Z., Sun, L.M., Huang, Y.J., Wang, Y.Z., Zhang, M.J., 2016. Nat. Nanotechnol. 11, 388–394.

Gendler, S.J., 2001. J. Mammary Gland Biol. Neoplas. 6, 339–353.

Hu, Y., Zhang, Q., Guo, Z., Wang, S., Du, C., Zhai, C., 2017. Biosens. Bioelectron. 98, 91–99.

Huang, Q., Wang, Y., Chen, X., Wang, Y., Li, Z., Du, S., Wang, L., Chen, S., 2018. Nanotheranostics 2, 21–41.

Jiang, H., Xu, G., Sun, Y., Zheng, W., Zhu, X., Wang, B., Zhang, X., Wang, G., 2015. Chem. Commun. 51, 11810–11813.

Joosse, S.A., Gorges, T.M., Pantel, K., 2015. EMBO Mol. Med. 7, 1–11.

Kelley, L.C., Wang, Z., Hagedorn, E.J., Wang, L., Shen, W., Lei, S., Johnson, S.A., Sherwood, D.R., 2017. Nat. Protoc. 12, 2081–2096.

Kim, H., Yoon, S.C., Lee, T.Y., Jeong, D., 2009. Toxicol. Lett. 184, 13–17.

Koren, S., Bentires-Alj, M., 2015. Mol. Cell. 60, 537–546.

Li, C., Heidt, D.G., Dalerba, P., Burant, C.F., Zhang, L., Adsay, V., Wicha, M., Clarke, M.F., Simeone, D.M., 2007. Cancer Res. 67, 1030–1037.

Li, D., Qiao, Z., Yu, Y., Tang, J., He, X., Shi, H., Ye, X., Lei, Y., Wang, K., 2018. Chem. Commun. 54, 1089–1092.

Maheswaran, S., Haber, D.A., 2015. Cancer Res. 75, 2411–2415.

Miao, P., Wang, B., Chen, X., Li, X., Tang, Y., 2015. ACS Appl. Mater. Inter. 7, 6238–6243.

Mishra, S.K., Srivastava, A.K., Kumar, D., Biradar, A.M., Rajesh, 2013. Nanoscale 5, 10494–10503.

Mohme, M., Riethdorf, S., Pantel, K., 2017. Nat. Rev. Clin. Oncol. 14, 155–167.

Nath, S., Mukherjee, P., 2014. Trends Mol. Med. 20, 332–342.

Peng, X., Zhu, J., Wen, W., Bao, T., Zhang, X., He, H., Wang, S., 2018. Biosens. Bioelectron. 118, 174–180.

Steel, A.B., Herne, T.M., Tarlov, M.J., 1998. Anal. Chem. 70, 4670–4677.

Stoecklein, N.H., Fischer, J.C., Niederacher, D., Terstappen, L.W., 2016. Expert Rev. Mol. Diagn. 16, 147–164.

Sun, D., Lu, J., Luo, Z., Zhang, L., Liu, P., Chen, Z., 2018. Biosens. Bioelectron. 120, 8–14.

Tan, W.H., Donovan, M.J., Jiang, J.H., 2013. Chem. Rev. 113, 2842–2862.

Tao, Z., Dang, X., Huang, X., Muzumdar, M.D., Xu, E.S., Bardhan, N.M., Song, H., Qi, R., Yu, Y., Li, T., Wei, W., Wyckoff, J., Birrer, M.J., Belcher, A.M., Ghoroghchian, P.P., 2017. Biomaterials 134, 202–215.

Wan, Y., Zhou, Y.G., Poudineh, M., Saberi Safaei, T., Mohamadi, R.M., Sargent, E.H., Kelly, S.O., 2014. Angew. Chem. Int. Ed. 53, 13145–13149.

Wolfson, E., Solomon, S., Schmukler, E., Goldshmit, Y., Pinkas-Kramarski, R., 2018. Cell Death Dis. 9, 47.

Wu, M.S., Yuan, D.J., Xu, J.J., Chen, H.Y., 2013. Anal. Chem. 85, 11960–11965.

Zhang, F.L., Jiang, Y., Liu, X.L., Meng, J.X., Zhang, P.C., Liu, H.J., Yang, G., Li, G.N., Jiang, L., Wan, L.J., Hu, J.S., Wang, S.T., 2016. Nano Lett. 16, 766–772.

Zhang, X., Qian, Y., Ma, X., Xia, M., Li, S., Zhang, Y., 2018. Nanoscale 10, 76–81.

Zhao, J., Tang, Y., Cao, Y., Chen, T., Chen, X., Mao, X., Yin, Y., Chen, G., 2018. Electrochim. Acta 283, 1072–1078.

Zhu, J., Zhang, L., Teng, Y., Lou, B., Jia, X., Gu, X., Wang, E., 2015. Nanoscale 7, 13224–13229.